

## STRUCTURE NOTE

# Crystal structure of a 3-oxoacyl-(acyl carrier protein) reductase (BA3989) from *Bacillus anthracis* at 2.4-Å resolution

Nathan R. Zaccai,<sup>1</sup> Lester G. Carter,<sup>1</sup> Nick S. Berrow,<sup>1</sup> Sarah Sainsbury,<sup>1</sup> Joanne E. Nettleship,<sup>1</sup> Thomas S. Walter,<sup>1</sup> Karl Harlos,<sup>1</sup> Ray J. Owens,<sup>1</sup> Keith S. Wilson,<sup>2</sup> David I. Stuart,<sup>1</sup> and Robert M. Esnouf<sup>1\*</sup>

<sup>1</sup>The Oxford Protein Production Facility, Division of Structural Biology, University of Oxford, Roosevelt Drive, Oxford, OX3 7BN, United Kingdom

<sup>2</sup>York Structural Biology Laboratory, Department of Chemistry, University of York, Heslington, York YO10 5YW, United Kingdom

**Key words:**  $\beta$ -ketoacyl-(acyl carrier protein)reductase; short-chain dehydrogenase/reductase (SDR); FabG; fatty acid biosynthesis; X-ray crystallography.

## INTRODUCTION

The Oxford Protein Production Facility (OPPF) was established to develop methods for high-throughput protein production and crystallization. As part of these developments, and in the context of the European SPINE project, a pilot study was undertaken on 48 proteins from *Bacillus anthracis* from protein families which were well conserved across a wide range of bacteria.<sup>1,2</sup> *Bacillus anthracis*, the causative agent of anthrax, is a large, gram-positive, spore-bearing bacterium. The genome of the Ames strain of the bacterium has been sequenced<sup>3</sup> showing two plasmids, pXO1 and pXO2, that carry the major virulence factors, as well as normal chromosomal DNA of 5.23 megabases, predicted to code for about 5311 genes. The set of 48 proteins chosen for study<sup>1</sup> are all encoded for by the chromosomal DNA.

Annotation of the *B. anthracis* genome suggests it encodes for four or five 3-oxoacyl-[acyl carrier protein (ACP)] reductases. These form part of the  $\beta$ -ketoacyl-(ACP) reductase family, itself part of the short-chain dehydrogenase/reductase (SDR) superfamily, whose members catalyze a broad range of reactions using nucleotide cofactors. This study reports the structure of gene product BA3989, a 3-oxoacyl-(ACP) reductase of 246 residues, determined to a resolution of 2.4 Å using protein produced by the high-throughput pipeline of the OPPE. This enzyme performs the first reductive step in *de novo* fatty-

acid biosynthesis<sup>4</sup>: the pyridine-nucleotide-dependent reduction of a 3-oxoacyl form of ACP (Fig. 1). Fatty-acid biosynthesis occurs by a series of universal biochemical transformations that are critical to almost all cells, but the pathway followed by bacterial systems differs substantially from that of higher organisms. Since this pathway is predicted to be essential<sup>5</sup> it has been suggested as an attractive target for the development of novel antibiotics.<sup>6–8</sup> Although to date no antibiotics target 3-oxoacyl-(ACP) reductases, a possible lead compound, epigallocatechin gallate from green tea, has been shown to be a potent inhibitor of the *Escherichia coli* oxoacyl reductase FabG.<sup>9</sup>

F1

## MATERIALS AND METHODS

Cloning, expression and purification followed standard OPPE pipeline protocols.<sup>2,10,11</sup> Briefly, the expression

Grant sponsor: UK Medical Research Council, MRC; Grant sponsor: SPINE; Grant number: QLG2-CT-2002-00988.

Nathan R. Zaccai's current address is Department of Pharmacology, University of Bristol, University Walk, Bristol BS8 1TD, UK.

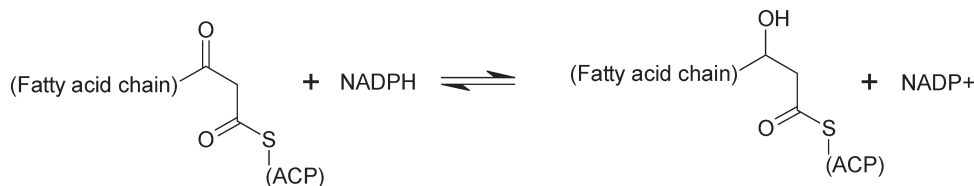
Lester G. Carter's current address is Centre for Biomolecular Sciences, University of St. Andrews, North Haugh, St Andrews, KY16 9ST, UK.

\*Correspondence to: Dr. Robert Esnouf, Division of Structural Biology, University of Oxford, Henry Wellcome Building for Genomic Medicine, Roosevelt Drive, Oxford, OX3 7BN, UK. E-mail: robert@strubi.ox.ac.uk

Received 13 March 2007; Accepted 26 March 2007

Published online 00 Month 2007 in Wiley InterScience (www.interscience.wiley.com). DOI: 10.1002/prot.21624

AQ2

**Figure 1**

Schematic of the reaction catalyzed by 3-oxoacyl-(ACP) reductase.

construct was generated by ligation-independent cloning using Gateway<sup>TM</sup> technology (Invitrogen). The BA3989 gene was amplified from genomic DNA with KOD HiFi<sup>TM</sup> polymerase (Novagen) using the forward primer 5'-ggggacaagttgtacaaaaagcaggcttctggaagtctgtccagggc-ccgATGTTAAAAGGGAAAGTAGCATTAGTAACGGGC-3' and the reverse primer 5'-ggggaccactttgtacaagaaagctgggtc tcaTTACATTACCATAACGCCATCAACATTTAACG-3'. The PCR product was purified using QIAquick 96 plates (Qiagen) and recombined with pDONR221 in the BP reaction. The insert from this vector was then transferred in the LR reaction to the expression vector pET15g which added a histidine purification tag and a 3C protease-cleavage site (underlined), MGSSHHHHHSSGLVPRG-SQSTSLYKKAGFLEVLQ↓GP, to the N terminus of the full length protein.<sup>12</sup> Recombinant LR clones were identified by PCR using a gene-specific forward primer, a T7 reverse primer and verified by sequencing. Protein was expressed in *E. coli* B834(DE3) cells grown at 37°C in GS96 media (QBiogene) to an A<sub>600</sub> of 0.6, induced with isopropyl β-D-thiogalactopyranoside (IPTG) to 0.5 mM and then incubated for a further 20 h at 20°C. Cells were harvested by centrifugation at 6000g for 15 min and lysed using a Basic-Z Cell Disruptor (Constant Systems Ltd) at 30 Kpsi in 50 mM Tris pH 7.5, 500 mM NaCl, 20 mM Tris and 0.2% Tween-20. Soluble protein was purified by nickel-affinity chromatography followed by size-exclusion chromatography on an akta 3D<sup>TM</sup> (GE Healthcare). Protein-containing fractions were analysed by SDS-PAGE (Criterion-Biorad). The purification tag was removed by overnight incubation at 4°C with His-tagged 3C protease (prepared from pET-24/His-3C kindly provided by A. Geerlof, EMBL Heidelberg, Germany) with the protease and any uncleaved protein being removed by nickel-affinity chromatography. The protein was concentrated to 9.7 mg/mL using a 5 K MWCO Vivaspine 15 concentrator (Vivascience) in 20 mM Tris pH 7.5, 200 mM NaCl and 1 mM Tris(2-carboxyethyl)phosphine hydrochloride (TCEP).

Crystallization trials used the OPF standard nanolitre crystallization protocol with standard OPF screens.<sup>13–15</sup> Crystals grew in Hampton Index condition 88: polyethylene glycol 3350 20% (w/v) and 0.2M triammonium citrate pH 7.0 (Hampton Research).

X-ray data were collected on station 14.1 at the Synchrotron Radiation Source (Daresbury, UK) from a crystal maintained at 100 K using an ADSC Quantum 4 detector. A total of 392 images were recorded using 0.5° oscillations, 20-s exposures and a crystal-to-detector distance of 135 mm. Prior to flash cooling, the crystal was protected by soaking briefly in perfluoropolyether XR-75 oil (Interchim). Data were indexed, integrated and reduced using DENZO and SCALEPACK<sup>16</sup> (Table I).

The structure was determined by molecular replacement using AMoRe<sup>17</sup> and the tetramer of *E. coli* β-

T1

**Table I**

Summary of Crystal Parameters, Data Collection, Model, and Refinement Statistics

<b>Data collection</b>	
Beam line	SRS Daresbury, Station 14.1
Space group	$P2_1$
Unit-cell parameters (Å, °)	$a = 70.6, b = 120.7,$ $c = 136.4, \beta = 104.4$
Wavelength (Å)	1.488
Resolution range (Å)	30–2.4 (2.49–2.4)
Number of observations	12,10,675
Number of unique reflections	82,223
Completeness (%)	94.3 (64.5)
Mean $I/\sigma(I)$	9.0 (1.6)
Redundancy	3.1 (1.5)
$R_{\text{merge}}^a$	0.150 (0.553)
<b>Model and refinement statistics</b>	
Resolution range (Å)	30–2.4 (2.46–2.4)
Number of reflections (work set)	77,199 (3687)
Number of reflections (test set)	4130 (175)
$R_{\text{cryst}}^b$	0.180 (0.263)
$R_{\text{free}}^c$	0.225 (0.326)
Number of non-H atoms (protein/water)	14,624/575
<b>Stereochemical parameters</b>	
RMS bond length deviation (Å)	0.013
RMS bond angle deviation (°)	1.3
Mean $B$ value (Å <sup>2</sup> )	47.9
Residues in allowed Ramachandran regions (%) <sup>d</sup>	99.4

Values in parenthesis refer to the specified outer resolution shell.

<sup>a</sup> $R_{\text{merge}} = \sum |I - \langle I \rangle| / \sum \langle I \rangle$ .

<sup>b</sup> $R_{\text{cryst}} = \sum |F_{\text{obs}} - F_{\text{calc}}| / \sum F_{\text{obs}}$ .

<sup>c</sup> $R_{\text{free}}$  is defined as for  $R_{\text{cryst}}$  but based on 5% of the total reflections chosen at random and omitted from the refinement.

<sup>d</sup>As defined by MolProbity. The percentages of residues having most favoured, additionally allowed, generously allowed and disallowed conformations (using the Procheck definitions) are 90.0, 9.4, 0.4, and 0.2%, respectively.

ketoacyl-(ACP) reductase (PDB ID 1Q7C; Ref. 18) as the search model. Initial refinement and rebuilding used CNS<sup>19</sup> and O,<sup>20</sup> while the final cycles used REFMAC<sup>21</sup> and Coot.<sup>22</sup> Non-crystallographic restraints were kept tight throughout refinement, although restraints were removed from residues having different conformations in different chains (a total of 34 residues including the poorly ordered loop from 189–203), and TLS refinement was applied using each chain as a separate group.

Structures were analyzed using MolProbity,<sup>23</sup> DALI,<sup>24</sup> and PISA.<sup>25</sup> Structure superpositions were performed with SHP,<sup>26</sup> the sequence alignment used ESPript<sup>27</sup> and other figures were prepared using BobScript<sup>28</sup> and Raster3D.<sup>29</sup> Atomic coordinates (2uvd) and structure factors (r2uvdsf) have been deposited with the Protein Data Bank (PDB).

## RESULTS

The structure of a 3-oxoacyl-(ACP) reductase (EC 1.1.1.100) from *B. anthracis* has been determined to a resolution of 2.4 Å. The final model contains two tetramers displaying 222 symmetry (all chains are completely traced, although for some chains the electron density for residues 189–203 is poor) and 575 water molecules in the crystallographic asymmetric unit, but no bound cofactors or substrates. The model has a working *R* factor of 0.180 (free *R* factor of 0.225; Table I). Typically, there is a 0.2 Å root-mean-square (RMS) C $\alpha$ -atom deviation between pairs of chains. The quality of the model (summarized in Table I) is good with an RMS deviation in bond lengths of 0.013 Å and 99.4% of residues in the allowed regions of the Ramachandran plot (as defined in MolProbity).

Each chain comprises 10  $\alpha$ -helices (although helices  $\alpha$ 5 and  $\alpha$ 10 are kinked at residues Leu114 and Ser227, respectively) flanking a central seven-stranded parallel  $\beta$ -sheet forming an NAD(P)-binding Rossmann-like domain typical of SDRs [Fig. 2(A,B)]. The DALI server reveals close structural similarity to many other SDRs, for example, a RMS deviation of 1.6 Å over 242 aligned C $\alpha$  atoms for *Magnaporthe grisea* trihydroxynaphthalene reductase (PDB ID 1YBV; Ref. 30; 37% sequence identity). The highest levels of sequence identity in the PDB are to *E. coli* 3-oxoacyl-(ACP) reductase (PDB ID 1I01; Ref. 31; 56% identity) and *C. thermocellum* glucose-ribitol dehydrogenase (PDB ID 2HQ1; unpublished; 53% identity). However, these structures have no bound cofactors so the discussion below focuses on a comparison with the complex of *Brassica napus*  $\beta$ -keto-(ACP) reductase with NADP+ [PDB ID 1EDO; Ref. 32; RMS deviation of 0.9 Å over 241 aligned C $\alpha$  atoms using SHP; 52% sequence identity; Fig. 2(B,C)].

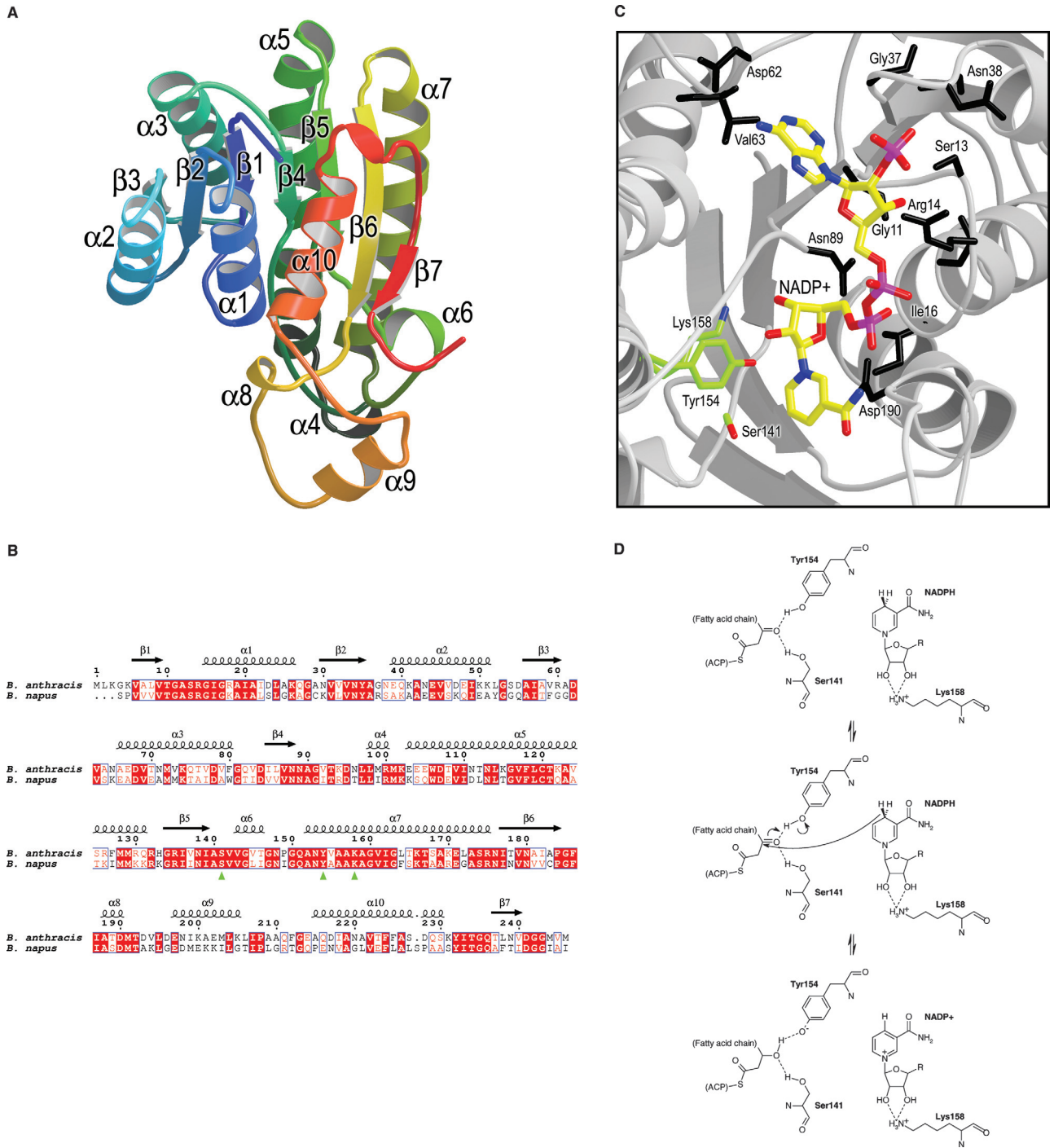
Analysis of the crystal packing (using PISA) indicates that, in common with other 3-oxoacyl-(ACP) reductases, the tetramer is the biologically active form. The tetramer

measures  $\sim$ 85 Å across and contains two types of dimerization interface. One interface ( $\sim$ 1600 Å<sup>2</sup>) comprises residues 98–107 (parts of helices  $\alpha$ 4 and  $\alpha$ 5) and residues 145–171 (parts of helices  $\alpha$ 6 and  $\alpha$ 7) from adjacent monomers. The interactions involving helices  $\alpha$ 4 and  $\alpha$ 5 are almost exclusively hydrophobic, although Lys115 makes salt bridges across to Glu103 and Asp107. In contrast, the interactions involving helices  $\alpha$ 6 and  $\alpha$ 7 contain several hydrogen bonds. The second interface ( $\sim$ 1350 Å<sup>2</sup>) comprises the C-terminal regions (residues 166–246) of two monomers. In particular, residues 211–220 from one chain make a number of hydrogen bonds and salt bridges with residues 229–232 from the other.

## DISCUSSION

This structure of *B. anthracis* 3-oxoacyl-(ACP) reductase contains no bound cofactor/substrate, but the active site can be compared with the superposed structure of the NADP+/ $\beta$ -keto-(ACP) reductase complex from *B. napus* [Fig. 2(C)]. The hydrogen bond network stabilizing the NADP+ would be expected to be similar to one in the *B. napus* complex. Based on this, the adenine ring would make direct hydrogen bonds between the nitrogen N1 and the amide hydrogen of Val63, and also between nitrogen N6 and the side chain of Asp62. The 3' adenine ribose hydroxyl would form direct hydrogen bonds to the side chain of Ser13, the carbonyl oxygen of Gly11 and the amide hydrogen of Arg14 (whose side chain would be displaced on binding). The 2' adenine ribose hydroxyl would hydrogen bond to the side chain of Ser13 and the phosphate group would interact with the side chain of Ser13 and the amide hydrogens of Gly37 and Asn38 (this loop is somewhat disordered in the *B. anthracis* structure and may only become properly ordered in the presence of the cofactor).

The *B. napus* structure suggests that on binding NADP+, several waters, which occupy the putative pyrophosphate-binding pocket in our structure, would be displaced and the pyrophosphate moiety would form hydrogen bonds to main chain atoms of Ile16, the side chain of Thr189 and, mediated by water, to the carbonyl oxygen of Arg14. The *B. anthracis* NADP+ binding pocket is ordered prior to binding, unlike the *E. coli*  $\beta$ -ketoacyl-(ACP)-reductase structure (PDB ID 1I01). The binding of the nicotinamide group would be stabilized by the protein main chain, whose conformation is largely similar to that observed in other NADP+/oxido-reductase complexes. A weak feature in our electron-density map appears to indicate the putative position of NO<sub>3</sub><sup>\*</sup>, which would make hydrogen bonds to the main chain of Asn89 and side chain of Lys158 (part of the catalytic triad). However, the region between residues 190–200 is poorly ordered, variable between the different chains in our model and differs significantly from the conformation



COLOR

**Figure 2**

Structure of 3-oxoacyl-(ACP) reductase. (A) The overall structure of the monomer. The model is coloured from blue at the N-terminus to red at the C-terminus and secondary structural elements are labelled. (B) Sequence alignment of *B. anthracis* 3-oxoacyl-(ACP) reductase (top) with its homologue from *Brassica napus*. Conserved residues are highlighted in red and the catalytic Ser-Tyr-Lys triad is indicated by green triangles. Residue numbering and secondary structural elements relate to the *B. anthracis* enzyme. (C) A model for the active site of *B. anthracis* 3-oxoacyl-(ACP) reductase showing the proposed binding mode for NADP<sup>+</sup>. The position of the cofactor was inferred by superposition of the *B. anthracis* and *B. napus* (PDB ID 1ED0) structures. The secondary structure of the *B. anthracis* enzyme is shown in grey with residues predicted to interact with NADP<sup>+</sup> shown as black sticks. NADP<sup>+</sup> is shown as atom-coloured sticks with yellow carbon atoms and the catalytic triad is shown as atom-coloured sticks with green carbon atoms. (D) The proposed reaction mechanism showing the role of the catalytic triad in facilitating hydride transfer from NADPH.

found in NADP<sup>+</sup> bound oxido-reductases. The side chain of Asp190 is positioned to interact with the pyrophosphate moiety, although for nicotinamide binding the residue would have to be displaced to prevent a steric clash.

Based on the analysis of the *B. napus* structure and mechanistic studies<sup>33</sup> the following mechanism is suggested [Fig. 2(D)]. In the first step, the phenolic group of Tyr154 residue forms a hydrogen bond with the carbonyl group of the 3-oxoacyl-(ACP). The hydroxyl group of Ser141 stabilizes this complex, helping to increase the polarization of the carbonyl group. The main role of Lys158 appears to be the stabilization of the nicotinamide ribose moiety of the NADPH through hydrogen bonds to the 2'-hydroxyl and 3'-hydroxyl groups. The NADPH is then involved in hydride transfer to the carbonyl carbon (becoming NADP<sup>+</sup> in the process) and proton transfer from Tyr154 completes the reaction. Alternatively, Lys158 may be more actively involved in the reaction by forming part of a "proton relay" which helps replenish Tyr154 mediated by the 2'-hydroxyl of the nicotinamide ribose moiety of the NADP(H).

## REFERENCES

- Au K, Berrow NS, Blagova E, Boucher IW, Boyle MP, Brannigan JA, Carter LG, Dierks T, Folkers G, Grenha R, Harlos K, Kaptein R, Kalliomaak AK, Levdikov VM, Meier C, Milioti N, Moroz O, Müller A, Owens RJ, Rzechorzek N, Sainsbury S, Stuart DI, Walter TS, Waterman DG, Wilkinson AJ, Wilson KS, Zaccari N, Esnouf RM, Fogg MJ. Application of high-throughput technologies to a structural proteomics-type analysis of *Bacillus anthracis*. *Acta Crystallogr* 2006;D62:1267–1275.
- Meier C, Carter LG, Winter G, Owens RJ, Stuart DI, Esnouf RM. Structure of 5-formyltetrahydrofolate cyclo-ligase from *Bacillus anthracis* (BA4489). *Acta Crystallogr* 2007;F63:168–172.
- Read TD, Peterson SN, Tourasse N, Baillie LW, Paulsen IT, Nelson KE, Tettelin H, Fouts DE, Eisen JA, Gill SR, Holtzapple EK, Okstad OA, Helgason E, Rilstone J, Wu M, Kolonay JF, Beanan MJ, Dodson RJ, Brinkac LM, Gwinn M, DeBoy RT, Madpu R, Daugherty SC, Durkin AS, Haft DH, Nelson WC, Peterson JD, Pop M, Khouri HM, Radune D, Benton JL, Mahamoud Y, Jiang L, Hance IR, Weidman JF, Berry KJ, Plaut RD, Wolf AM, Watkins KL, Nierman WC, Hazen A, Cline R, Redmond C, Thwaite JE, White O, Salzberg SL, Thomason B, Friedlander AM, Koehler TM, Hanna PC, Kolsto AB, Fraser CM. The genome sequence of *Bacillus anthracis* Ames and comparison to closely related bacteria. *Nature* 2003;423:81–86.
- Toomey RE, Wakil SJ. Studies on the mechanism of fatty acid synthesis. XV. Preparation and general properties of  $\beta$ -ketoacyl acyl carrier protein reductase from *Escherichia coli*. *Biochim Biophys Acta* 1966;116:189–197.
- Zhang Y, Cronan JE, Jr. Transcriptional analysis of essential genes of the *Escherichia coli* fatty acid biosynthesis gene cluster by functional replacement with the analogous *Salmonella typhimurium* gene cluster. *J Bacteriol* 1998;180:3295–3303.
- Surolia A, Ramya TN, Ramya V, Surolia N. 'FAS't inhibition of malaria. *Biochem J* 2004;383:401–412.
- Ramya TN, Surolia N, Surolia A. Is the fatty acid synthesis pathway a good target for anti-malarial therapy? *IUBMB Life* 2005;57:371–373.
- Zhang YM, Lu YJ, Rock CO. The reductase steps of the type II fatty acid synthase as antimicrobial targets. *Lipids* 2004;39:1055–1060.
- Zhang YM, Rock CO. Evaluation of epigallocatechin gallate and related plant polyphenols as inhibitors of the FabG and FabI reductases of bacterial type II fatty-acid synthase. *J Biol Chem* 2004;279:30994–31001.
- Ren J, Sainsbury S, Berrow NS, Alderton D, Nettleship JE, Stammers DK, Saunders NJ, Owens RJ. Crystal structure of nitrogen regulatory protein IIANtr from *Neisseria meningitidis*. *BMC Struct Biol* 2005;10:13.
- Alzari PM, Berglund H, Berrow NS, Blagova E, Busso D, Cambillau C, Campanacci V, Christodoulou E, Eiler S, Fogg MJ, Folkers G, Geerlof A, Hart D, Haouz A, Herman MD, Macieira S, Nordlund P, Perrakis A, Quevillon-Cheruel S, Tarandeu F, van Tilbeurgh H, Unger T, Luna-Vargas MP, Velarde M, Willmanns M, Owens RJ. Implementation of semi-automated cloning and prokaryotic expression screening: the impact of SPINE. *Acta Crystallogr* 2006;D62:1103–1113.
- Luan CH, Qiu S, Finley JB, Carson M, Gray RJ, Huang W, Johnson D, Tsao J, Reboul J, Vaglio P, Hill DE, Vidal M, Delucas LJ, Luo M. High-throughput expression of *C. elegans* proteins. *Genome Res* 2004;14:2102–2110.
- Walter TS, Diprose J, Brown J, Pickford M, Owens RJ, Stuart DI, Harlos K. A procedure for setting up high-throughput nanolitre crystallization experiments. I. Protocol design and validation. *J Appl Crystallogr* 2003;36:308–314.
- Brown J, Walter TS, Carter L, Abrescia NGA, Aricescu AR, Batuwangala TD, Bird LE, Brown N, Chamberlain PP, Davis SJ, Dubinina E, Endicott J, Fennelly JA, Gilbert RJC, Harkiolaki M, Hon WC, Kimberley F, Love CA, Mancini EJ, Manso-Sancho R, Nichols CE, Robinson RA, Sutton GC, Schueller N, Sleeman MC, Stewart-Jones GB, Vuong M, Welburn J, Zhang Z, Stammers DK, Owens RJ, Jones EY, Harlos K, Stuart DI. A procedure for setting up high-throughput nanolitre crystallization experiments. II. Crystallization results. *J Appl Crystallogr* 2003;36:315–318.
- Walter TS, Diprose JM, Mayo CJ, Siebold C, Pickford MG, Carter L, Sutton GC, Berrow NS, Brown J, Berry IM, Stewart-Jones GB, Grimes JM, Stammers DK, Esnouf RM, Jones EY, Owens RJ, Stuart DI, Harlos K. A procedure for setting up high-throughput nanolitre crystallization experiments. Crystallization workflow for initial screening, automated storage, imaging and optimization. *Acta Crystallogr* 2005;D61:651–657.
- Otwinowski Z, Minor W. Processing of X-ray diffraction data collection in oscillation mode. *Methods Enzymol* 1997;276:307–326.
- Navaza J, Saludjian P. AMoRe: An automated molecular replacement program package. *Methods Enzymol* 1997;276:581–594.
- Price AC, Zhang YM, Rock CO, White SW. Cofactor-induced conformational rearrangements establish a catalytically competent active site and a proton relay conduit in FabG. *Structure (Camb)* 2004;12:417–428.
- Brünger AT, Adams PD, Clore GM, DeLano WL, Gros P, Grosse-Kunstleve RW, Jiang JS, Kuszewski J, Nilges M, Pannu NS, Read RJ, Rice LM, Simonson T, Warren GL. Crystallography and NMR system: a new software suite for macromolecular structure determination. *Acta Crystallogr* 1998;D54:905–921.
- Jones TA, Zhou JY, Cowan SW, Kjeldgaard M. Improved methods for building protein models in electron density maps and the location of errors in these models. *Acta Crystallogr* 1991;A47:110–119.
- Murshudov GN, Vagin AA, Lebedev A, Wilson KS, Dodson EJ. Efficient anisotropic refinement of macromolecular structures using FFT. *Acta Crystallogr* 1999;D55:247–255.
- Emsley P, Cowtan K. Coot: model-building tools for molecular graphics. *Acta Crystallogr* 2004;D60:2126–2132.
- Lovell SC, Davis IW, Arendall WB III, de Bakker PI, Word JM, Prisant MG, Richardson JS, Richardson DC. Structure validation by C $\alpha$  geometry: phi, psi, and C $\beta$  deviation. *Proteins* 2003;50:437–450.
- Holm L, Sander C. Protein structure comparison by alignment of distance matrices. *J Mol Biol* 1993;233:123–138.

AQ1

25. Krissinel E, Henrick K. Detection of protein assemblies in crystals. In: Berthold MR, *et al.* editors. *CompLife 2005 Proceedings*. Berlin/Heidelberg: Springer-Verlag; 2005. pp 163–174.
26. Stuart DI, Levine M, Muirhead H, Stammers DK. Crystal structure of cat muscle pyruvate kinase at a resolution of 2.6 Å. *J Mol Biol* 1979;134:109–142.
27. Gouet P, Courcelle E, Stuart DI, Métoz F. ESPript: analysis of multiple sequence alignments in PostScript. *Bioinformatics* 1999;15:305–308.
28. Esnouf RM. Further additions to MolScript version 1.4, including reading and contouring of electron-density maps. *Acta Crystallogr* 1999;D55:938–940.
29. Merritt EA, Bacon DJ. Raster3D: photorealistic molecular graphics. *Methods Enzymol* 1997;277:505–524.
30. Andersson A, Jordan D, Schneider G, Lindqvist Y. Crystal structure of the ternary complex of 1,3,8-trihydroxynaphthalene reductase from *Magnaporthe grisea* with NADPH and an active-site inhibitor. *Structure* 1996;4:1161–1170.
31. Price AC, Zhang YM, Rock CO, White SW. Structure of beta-ketoacyl-[acyl carrier protein] reductase from *Escherichia coli*: negative cooperativity and its structural basis. *Biochemistry* 2001;40: 12772–12781.
32. Fisher M, Kroon JT, Martindale W, Stuitje AR, Slabas AR, Rafferty JB. The X-ray structure of *Brassica napus* beta-keto acyl carrier protein reductase and its implications for substrate binding and catalysis. *Struct Fold Des* 2000;8:339–347.
33. Tanaka N, Nonaka T, Nakamura KT, Hara A. SDR: structure, mechanism of action, and substrate recognition. *Curr Org Chem* 2001; 5:89–111.



Author Proof

AQ1: Kindly provide all the editor names for this reference.

AQ2: Kindly check whether the grant information is OK as typeset.



**Author Proof**